ELSEVIER

Dynamics of Atmospheres and Oceans 27 (1997) 175–185

dynamics of atmospheres and oceans

The poleward propagation of atmospheric angular momentum with a 30–60-day time scale

Tsing-Chang Chen *, Shu-Ping Weng

Atmospheric Science Program, Department of Geological and Atmospheric Sciences, 3010 Agronomy Hall, Iowa State University, Ames, IA 50011, USA

Received 22 December 1995; revised 11 September 1996; accepted 16 October 1996

Abstract

The existence of the intraseasonal variation of relative atmospheric angular momentum and the poleward propagation of this physical quantity by the intraseasonal mode of atmospheric circulation have been amply demonstrated in previous studies. However, the temporal relationship between the intraseasonal variation and poleward propagation is not well understood and the possible mechanism causing the poleward propagation is unknown. Analyzing the 15-year (1979–1993) upper-air data of the National Meteorological Center (currently the National Centers for Environmental Prediction), we explored these two intriguing issues related to atmospheric angular momentum via case-study analyses. The major findings are as follows:

1. The maximum (minimum) 30–60-day globally integrated atmospheric angular momentum occurs when the positive (negative) angular momentum anomalies of a 30–60-day cycle appear in the tropics–subtropics and those of the previous 30–60-day cycle propagate to the northern and southern midlatitudes.
2. The eastward propagation of the 30–60-day global divergent circulation induces a 30–60-day flip–flop oscillation in the meridional circulation which in turn results in a similar alternation in the angular momentum tendency caused by the Coriolis torque. It was inferred from the zonal-mean angular momentum budget analysis that the 30–60-day variation of atmospheric angular momentum and its poleward propagation are results of the 30–60-day variation of the aforementioned momentum tendency.

1. Introduction

Lambeck and Cazenave (1974) found an intraseasonal variation in the length of day (LOD) caused by changes in the atmospheric relative angular momentum (RAM). Their

* Corresponding author.

0377-0265/97/$17.00
PII S0377-0265(97)00007-9

finding was later confirmed by Langley et al. (1981). A brief account of the coherent intraseasonal fluctuation between LOD and RAM can be found in reviews by Rosen (1993) and Madden and Julian (1994). Since the III-b FGGE (First Global GARP Experiment) data became available in the early 1980s, the intraseasonal oscillation of the tropical zonal wind originally detected by Madden and Julian (1971, 1972) has been the focus of numerous research efforts related to this low-frequency mode in the atmospheric circulation. In particular, a major concern has been the intraseasonal oscillation of RAM.

Correlating the RAM and the 40–50-day bandpass filtered zonal-mean wind, Anderson and Rosen (1983) showed that the RAM reaches its maximum when the upper-tropospheric zonal wind maximum moved poleward of 20°N and 20°S. Recently, Gutzler and Madden (1993) suggested with a cross-spectral analysis of RAM between the tropics and higher latitudes that there is a poleward propagation of RAM from the tropics, particularly during boreal winter. Kang and Lau (1994) isolated the principal mode of the atmospheric circulation associated with the intraseasonal variation of RAM and found the intensification of subtropical westerly flow following a weakening of the Hadley circulation. The intraseasonal variation of RAM may be linked to the intraseasonal oscillation of the Hadley circulation and this oscillation may be induced by the eastward propagation of the 30–60-day global divergent circulation (Lorenc, 1984, Krishnamurti et al., 1985, Chen et al., 1988). In view of these previous studies, some questions may be raised:

1. How is the intraseasonal variation of the globally integrated RAM related to the poleward propagation of RAM?
2. How is the poleward propagation of RAM coupled with the eastward propagation of the intraseasonal global divergent circulation through the meridional circulation?

In order to answer these questions, we analyzed the zonal-mean relative atmospheric angular momentum budget with the global 2.5° (longitude) × 2.5° (latitude) upper-air data generated by the Global Data Assimilation System of the National Meteorological Center (NMC) for the past 15 years (1979–1993). However, we present only some selected case analyses in this study.

2. Poleward propagation

For discussion, the atmospheric angular momentum relative to the Earth's surface is $m_r = ua\cos\phi$, and its zonal-mean value is $m_{rZ} = (1/2\pi)\int_0^{2\pi} m_r \mathrm{d}\lambda$. As done in numerous studies, the relative atmospheric angular momentum integrated between 1000 and 100 mb is

$$\begin{aligned} M_r &= (2\pi/g)\int_{100\text{ mb}}^{1000\text{ mb}}\int_{-\pi/2}^{\pi/2} m_{rZ}a^2\cos\phi\,\mathrm{d}\phi\,\mathrm{d}p \\ &= 2\pi\int_{-\pi/2}^{\pi/2}\langle m_{rZ}\rangle a^2\cos\phi\,\mathrm{d}\phi \end{aligned} \tag{1}$$

where $\langle(\,)\rangle \equiv (1/g)\int_{100\text{ mb}}^{1000\text{ mb}}(\,)\mathrm{d}p$. The notation used here is conventional; u, a, g, p and ϕ are zonal velocity, the Earth's radius, gravity, pressure and latitude, respectively.

The possible poleward propagation of relative atmospheric angular momentum by the intraseasonal model was demonstrated by Anderson and Rosen (1983) in terms of the latitude–height cross-section of correlation coefficient between the bandpass filtered M_r time series and the bandpass filtered zonal-mean wind anomalies. Recently, Gutzler and Madden (1993) used the cross-spectral analysis of the atmospheric angular momentum in the tropics and higher latitudes to infer this propagation. However, to obtain a direct view of the poleward propagation of atmospheric angular momentum by the 30–60-day mode and a relation between the 30–60-day (denoted by $\tilde{(\ )}$) variation of M_r and this propagation, the time series of $\tilde{M}_r$ and a latitude–time diagram of $\langle \tilde{m}_{rZ} \rangle$ over the time period of 8/29/91–5/1/92 are displayed in Fig. 1. The second-order Butterworth bandpass filter (Murakami, 1979) was adopted in this study to isolate the 30–60-day mode of all variables. Although we analyzed atmospheric angular momentum with the NMC data for a 15-year (1979–1993) period, the time period of 8/29/91–5/1/92 was randomly selected for focused study. The poleward propagation of $\langle \tilde{m}_{rZ} \rangle$ stands out

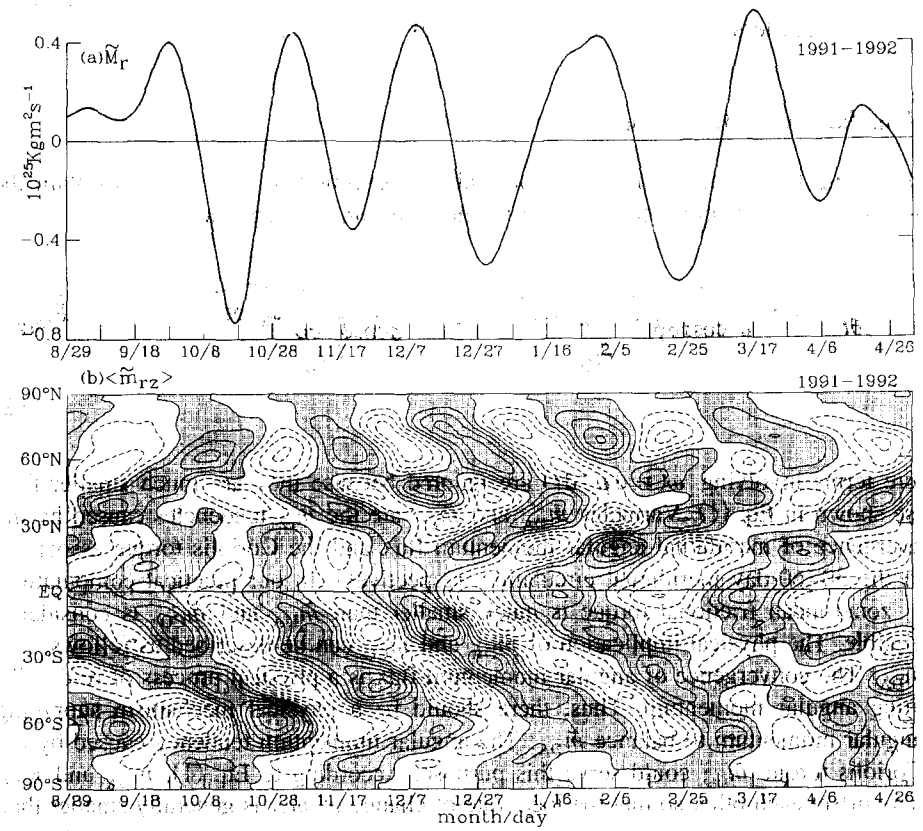

Fig. 1. (a) The time series of $\tilde{M}_r$ (30–60-day filtered globally integrated relative atmospheric angular momentum (M_r)), and (b) the $y-t$ diagram of $\langle \tilde{m}_{rZ} \rangle$ (the zonally averaged 30–60-day filtered relative atmospheric angular momentum integrated over the entire depth of atmosphere). The positive values of $\langle \tilde{m}_{rZ} \rangle$ in (b) are stippled. The contour interval of $\langle \tilde{m}_{rZ} \rangle$ is 2×10^{10} kg m^2 s^{-1}

clearly between 60°N and 60°S, and generally starts from the tropics. In high latitudes, particularly in the Northern Hemisphere, $\langle \tilde{m}_{rZ} \rangle$ exhibits an equatorward propagation. The poleward propagation of $\langle \tilde{m}_{rZ} \rangle$ was demonstrated by previous studies (e.g. Anderson and Rosen, 1983) but the latitude–time diagram of $\langle \tilde{m}_{rZ} \rangle$ provides an illustrative way of expressing this interesting phenomenon.

One of two questions with which this study is concerned is the relation between the intraseasonal variation of M_r and the poleward propagation of $\langle \tilde{m}_{rZ} \rangle$. This question can be answered by the contrast between the $\tilde{M}_r$ time series (Fig. 1(a)) and the latitude–time diagram of $\langle \tilde{m}_{rZ} \rangle$ (Fig. 1(b)). $\tilde{M}_r$ reaches its maximum (minimum) when $\langle \tilde{m}_{rZ} \rangle$ positive (negative) anomalies in a given 30–60-day cycle are migrating toward the subtropics of both hemispheres and those of the previous 30–60-day cycle, in opposite phase, arrive at midlatitudes. The Anderson and Rosen (1983) correlation coefficient patterns suggests that $\tilde{M}_r$ reaches its maximum (minimum) when positive (negative) $\langle \tilde{m}_{rZ} \rangle$ anomalies reach 20°N and 20°S. As revealed from its latitude–time diagram, the poleward propagation of the $\langle \tilde{m}_{rZ} \rangle$ in higher latitudes is not as regular and stable as in lower latitudes. It is likely then that the Anderson and Rosen (1983) correlation coefficients are less noticeable in higher latitudes for this reason.

3. Angular momentum budget

Applying the zonal-mean u equation and the definition of M_r, one can obtain the 30–60-day zonal-mean relative angular momentum $\langle \tilde{m}_{rZ} \rangle$ budget equation

$$\frac{\partial \tilde{m}_{rZ}}{\partial t} \simeq \underbrace{-\frac{1}{a\cos\phi\partial\phi}[\widetilde{(uv)}_Z a\cos^2\phi]}_{\tilde{m}_{DA}} + \underbrace{[f - \frac{1}{a\cos\phi}\frac{\partial}{\partial\phi}(\widetilde{u_Z\cos\phi})]v_Z a\cos\phi}_{\tilde{m}_{CO}} + \tilde{F}_{m_{rZ}}, \tag{2}$$

where terms involving $\omega(\equiv \mathrm{d}p/\mathrm{d}t)$ are ignored because they are much smaller than those shown in Eq. (1). Variables $\tilde{m}_{DA}$ and $\tilde{m}_{CO}$ are the $\tilde{m}_{rZ}$ tendencies caused by the convergence of meridional angular momentum flux and the Coriolis torque associated with the 30–60-day meridional circulation, respectively. In our practical computation, $\tilde{F}_{m_{rZ}}$ zonal-mean frictional torque is much smaller than $\tilde{m}_{DA}$ and $\tilde{m}_{CO}$, is considered negligible. The physical implication of $\tilde{m}_{DA}$ and $\tilde{m}_{CO}$ can be described as follows.

$\tilde{m}_{DA}$: The convergence of angular momentum flux is a physical process of re-distributing angular momentum. Thus, there should be a physical mechanism supplying angular momentum to balance $\tilde{m}_{DA}$. The angular momentum tendency caused by the Coriolis torque $\tilde{m}_{CO}$ could serve this purpose. According to Eq. (1), $\tilde{m}_{DA}$ and $\tilde{m}_{CO}$ may offset each other so that the local rate of change of $\tilde{m}_{rZ}$ is generally smaller than these two processes. Thus, the mutual adjustment between these two physical processes results in the change of angular momentum $\partial\tilde{m}_{rZ}/\partial t$.

$\tilde{m}_{CO}$: The quantity $f-(1/a\cos\phi)(\partial/\partial\phi)(u_Z\cos\phi)$ is the absolute vorticity of the basic flow. Except at the equator, the absolute vorticity of the basic flow is dominated

by planetary vorticity f (even in the tropics). Thus, the primary contribution to $\tilde{m}_{CO}$ is made primarily by the Coriolis torque. For this reason, any mechanism inducing a 30–60-day oscillation in the meridional circulation depicted with $\tilde{v}_Z$ certainly would result in a similar oscillation in $\tilde{m}_{CO}$. The most likely mechanism would be the eastward-propagating 30–60-day mode of the global divergent circulation. This issue will be elaborated further in Section 4.

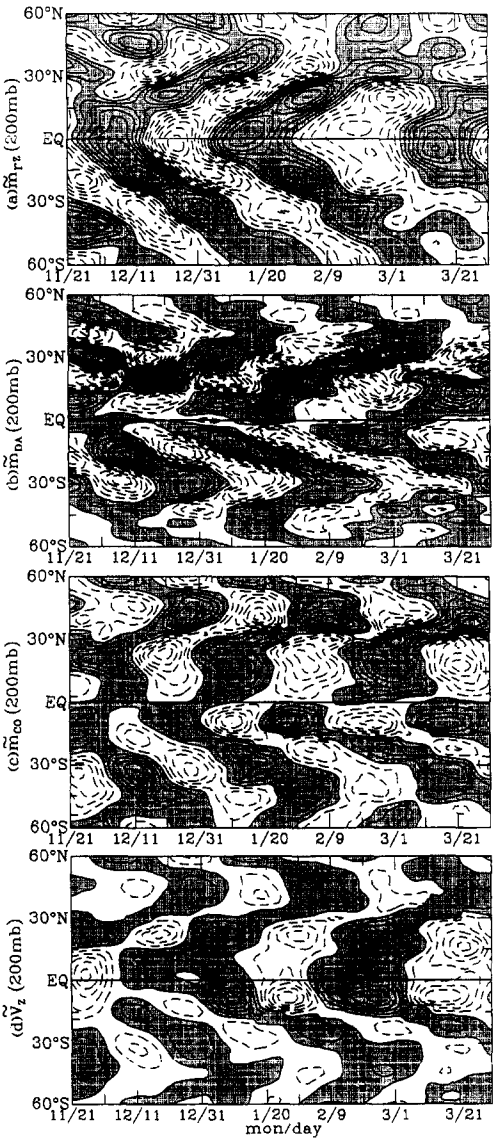

Fig. 2. The zonal-mean angular momentum ($\tilde{m}_{rZ}$(200 mb)) budget at 200 mb; (a) $\tilde{m}_{rZ}$(200 mb), (b) $\tilde{m}_{DA}$(200 mb), (c) $\tilde{m}_{CO}$(200 mb) and (d) $\tilde{v}_Z$(200 mb). Positive values of all variables are stippled. Contour intervals are: 3×10^6 m^2 s^{-1} for (a), 2×10^{-4} m^2 s^{-2} for (b) and (c), and 0.1 m s^{-1} for (d).

Displayed in Fig. 2 are the latitude–time diagrams of $\tilde{m}_{rZ}$, $\tilde{m}_{DA}$, $\tilde{m}_{CO}$ and $\tilde{v}_Z$ at 200 mb for a period (11/21/91–3/30/92) within the selected case-study period. The maintenance of $\tilde{m}_{rZ}$(200 mb) and poleward propagation will be illustrated with these latitude–time diagrams. The salient features of the $\tilde{m}_{rZ}$(200 mb) budget is highlighted as follows:

1. Although the maximum variance of $\tilde{m}_{rZ}$ exists in the upper troposphere, the $\tilde{m}_{rZ}$ anomalies of the same sign extend almost throughout the entire troposphere (refer to Fig. 3). Thus, the $\tilde{m}_{rZ}$(200 mb) budget reflects the $\tilde{m}_{rZ}$ maintenance over the entire troposphere. As revealed from the $\tilde{m}_{rZ}$(200 mb) latitude–time diagram, the poleward propagation of $\tilde{m}_{rZ}$(200 mb) during the period of 11/21/91–3/30/92 matches very well with the latitude–time diagram of $\langle \tilde{m}_{rZ} \rangle$ (Fig. 1(b)).

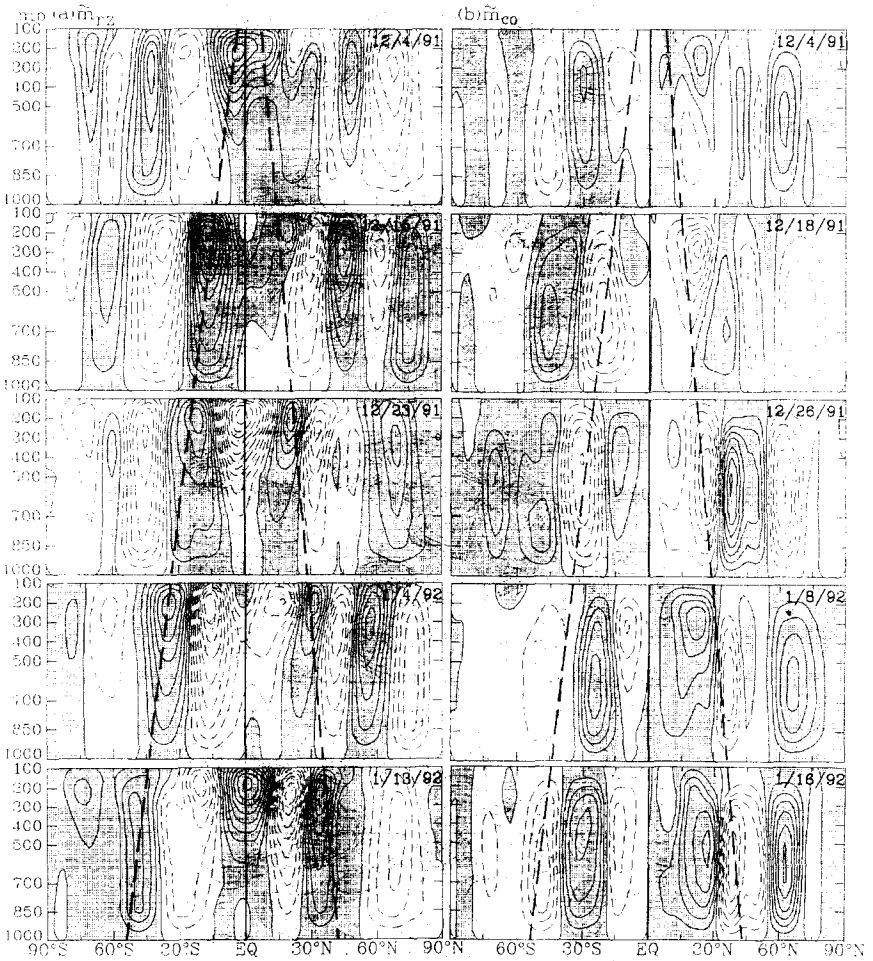

Fig. 3. Latitude–time cross-sections of (a) $\tilde{m}_{rZ}$ and (b) $\tilde{m}_{CO}$ for five phases of a 30–60-day cycle (12/4/91–1/13/92). Thick-dashed lines are drawn in the two hemispheres to indicate the coherent polarward propagation of $\tilde{m}_{rZ}$ and $\tilde{m}_{CO}$ anomalies. Positive values of these two quantities are stippled. Contour intervals of $\tilde{m}_{rZ}$ and $\tilde{m}_{CO}$ are 2×10^6 m^2 s^{-1} and 3×10^{-4} m^2 s^{-2}, respectively.

2. In practice, the computation of $\tilde{m}_{CO}(200\ \text{mb})$ is approximated by $f\tilde{v}_\chi(200\ \text{mb})a\cos\phi$. The latitude–time diagrams of both $\tilde{m}_{DA}(200\ \text{mb})$ (Fig. 2(b)) and $\tilde{m}_{CO}(200\ \text{mb})$ (Fig. 2(c)) are comparable in magnitude, but are opposite in sign. As inferred from Eq. (1), $\tilde{m}_{DA}(200\ \text{mb})$ and $\tilde{m}_{CO}(200\ \text{mb})$ should compensate for each other. Both $\tilde{m}_{DA}(200\ \text{mb})$ and $\tilde{m}_{CO}(200\ \text{mb})$ exhibit a poleward propagation coherent with that of $\tilde{m}_{tz}(200\ \text{mb})$; the $\tilde{m}_{tz}$ evolution apparently results from the mutual adjustment between $\tilde{m}_{DA}(200\ \text{mb})$ and $\tilde{m}_{CO}(200\ \text{mb})$.
3. It has been argued previously that $\tilde{m}_{CO}$ is a generating process of $\tilde{m}_{tz}$ and is approximated by $f\tilde{v}_\chi a\cos\phi$. Evidently, the 30–60-day variation of meridional circulation leads to a similar oscillation in $\tilde{m}_{CO}$, and in turn in $\tilde{m}_{tz}$. Thus, the 30–60-day variation of atmospheric angular momentum and its poleward propagation are linked to the 30–60-day oscillation of meridional circulation (as shown by the latitude–time diagram of $\tilde{v}_\chi$ in Fig. 2(d)) through $\tilde{m}_{CO}$. To support this argument, we display in Fig. 3 the $\tilde{m}_{tz}$ and $\tilde{m}_{CO}$ latitude–height cross-sections of five phases over a 30–60-day cycle (12/1/91–1/31/92). Superimposed on these cross-sections are thick-solid lines in the two hemispheres to indicate the poleward propagation of $\tilde{m}_{tz}$ and $\tilde{m}_{CO}$ anomalies. Note that the data quality of $\tilde{v}_\chi$ is generally limited by the operational global data assimilation system. However, even under this constraint, a coherent poleward propagation of $\tilde{m}_{tz}$ and the 30–60-day meridional circulation (inferred from $\tilde{m}_{CO}$) emerges from the contrast between $\tilde{m}_{tz}$ and $\tilde{m}_{CO}$ anomalies associated with thick-dashed lines connecting five consecutive panels of these two quantities.

4. Effect of the eastward-propagating 30–60-day mode

It has been shown by numerous studies (e.g. Lorenc, 1984, Krishnamurti et al., 1985, Knutson and Weickmann, 1987) that global velocity potential (χ) is a sensitive variable with which to portray the spatial structure and eastward propagation of the 30–60-day intraseasonal mode. Shown in Fig. 4 is the longitude–time diagram of $\tilde{\chi}(200\ \text{mb})$ at the equator for the period of 11/21/91–3/30/92. In addition to a relatively regular eastward propagation during this time period, the global $\tilde{\chi}(200\ \text{mb})$ field also exhibits a wavenumber-1 structure. For illustration, the horizontal charts of the 200-mb 30–60-day divergent circulation ($\tilde{\chi}$, $\tilde{V}_D$)(200 mb) are displayed in Fig. 5 at the dates of a maximum $\tilde{M}_r$ (1/27/92) and a minimum $\tilde{M}_r$ (2/22/92). During the maximum $\tilde{M}_r$ phase, the divergent center of ($\tilde{\chi}$, $\tilde{V}_D$)(200 mb) is located over Africa and the convergent center is over the Pacific. The spatial structure of the 30–60-day global divergent circulation is reversed during the minimum $\tilde{M}_r$ phase. The contrast of the global 30–60-day divergent circulation between the maximum and minimum $\tilde{M}_r$ phases shown in Fig. 4 is true for other cases, as determined from analysis of the full 15 years of NMC data. In other words, the contrast of ($\tilde{\chi}$, $\tilde{V}_D$)(200 mb) between the two extremes of $\tilde{M}_r$ revealed from this figure is a common feature to all cases over this 15-year period.

The second major concern of this study raised in Section 1 was how the eastward propagation of the 30–60-day global divergent circulation affects the $\tilde{M}_r$ variation. Let us recheck the latitude–time diagram of $\tilde{v}_\chi(200\ \text{mb})$ (Fig. 2(d)) on the two dates:

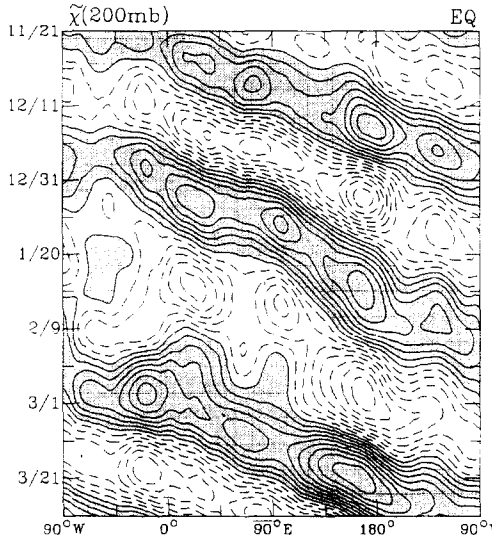

Fig. 4. The longitude–time diagram of $\tilde{\chi}$(200 mb) at the equator. Positive values of $\tilde{\chi}$(200 mb) are stippled. The contour interval of $\tilde{\chi}$(200 mb) is 7.5×10^5 m^2 s^{-1}.

1/27/92 (maximum $\tilde{M}_r$) and 2/22/92 (minimum $\tilde{M}_r$). Clearly, $\tilde{v}_Z$(200 mb) reaches its maximum negative (positive) values at the subtropics of both hemispheres during the maximum (minimum) $\tilde{M}_r$ phase. The relationship between $\tilde{v}_Z$(200 mb) anomalies and

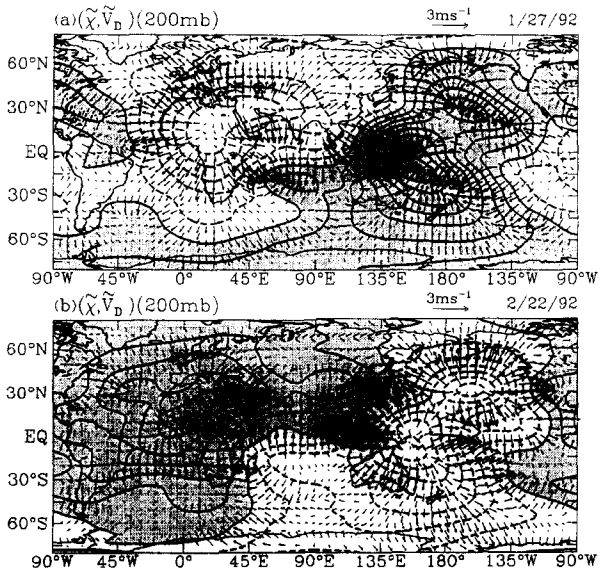

Fig. 5. The global charts of the 30–60-day filtered 200-mb divergent circulation ($\tilde{\chi}$, $\tilde{V}_D$)(200 mb) for (a) 1/27/92 (maximum $\tilde{M}_r$) and (b) 2/22/92 (minimum $\tilde{M}_r$). Positive values of $\tilde{\chi}$(200 mb) are stippled. The contour interval of $\tilde{\chi}$(200 mb) is 7.5×10^5 m^2 s^{-1}.

$\tilde{M}_r$ variation found here is consistent with that between the first eigenmodes of $\tilde{\psi}_m$ and the zonal-mean wind depicted by Kang and Lau (1994). The alternation of negative and positive $\tilde{v}_Z$(200 mb) between maximum and minimum $\tilde{M}_r$ results from the flip–flop oscillation of the 200-mb divergent circulation shown in Fig. 5. The contrast between the latitude–time diagram of $\tilde{v}_Z$(200 mb) (Fig. 2(d)) and the longitude–time diagram of $\tilde{\chi}$(200 mb) (Fig. 4) indicates that the alternation between the negative and positive $\tilde{v}_Z$(200 mb), namely the 30–60-day component of meridional circulation, is caused by the eastward propagation of the global 30–60-day divergent circulation. Recall that the 30–60-day angular momentum tendency generated by the Coriolis torque is induced by the 30–60-day component of meridional circulation (indicated by $\tilde{v}_Z$). It is inferred from these two reasons that the 30–60-day variation of M_r and the poleward propagation of $\langle \tilde{m}_{rZ} \rangle$ are related to the eastward propagation of the global 30–60-day divergent circulation through the induced 30–60-day component of the meridional circulation.

5. Concluding remarks

The 30–60-day signal is observed in different components of the atmospheric circulation. Thus, it is expected that the intraseasonal 30–60-day modes of different atmospheric circulation components are inherently linked in some way. In this study, we focus on an interesting example of this linkage: the intraseasonal variation of relative atmospheric angular momentum (RAM). Previous studies have found (a) a 30–60-day variation of globally integrated RAM ($\tilde{M}_r$), (b) a poleward propagation of RAM by the 30–60-day mode and (c) the eastward propagation of the 30–60-day global divergent circulation. However, the basic question facing us is how these different features of the 30–60-day mode are dynamically related. Analyzing 15 years (1979–1993) of upper-air data from the National Meteorological Center, we randomly selected the period 8/19/91–5/1/92 to illustrate the possible dynamic link between the three interesting features of the 30–60-day mode. The major findings are:

1. $\tilde{M}_r$ reaches its maximum (minimum) value when the positive (negative) RAM anomalies of a new 30–60-day cycle appear in the tropics–subtropics and when those of the previous 30–60-day cycle propagate to the midlatitudes of both hemispheres.
2. A 30–60-day oscillation of the meridional circulation is induced by the eastward propagation of the 30–60-day global divergent circulation.

The southward (northward) motion of the upper branch of the meridional circulation is formed in the tropics–subtropics when the upper divergent (convergent) center of the 30–60-day global divergent circulation is located over tropical Africa. In terms of the zonal-mean angular momentum budget, it is shown that the intraseasonal variation of the Coriolis torque in response to that of the meridional circulation is balanced by the convergence of angular momentum flux. The RAM poleward propagation by the 30–60-day mode results from the mutual adjustment between the aforementioned physical processes. Evidently, this RAM poleward propagation is induced by the eastward-propagating 30–60-day global divergent circulation through its link with the 30–60-day oscillation of the meridional circulation.

As suggested by the zonal-mean angular momentum budget analysis, the 30–60-day variation of M_r and the poleward propagation of relative atmospheric angular momentum by the 30–60-day mode are coupled with the eastward propagation of the 30–60-day global divergent circulation through the meridional circulation. Certainly, we hope that this suggestion can be substantiated through numerical experiments. As Madden and Julian (1994) pointed out, all numerical simulations of the global 30–60-day oscillation agree that hydrological processes are vital to the simulation of this intraseasonal oscillation. It is likely that the 30–60-day mode may be weaker or nonexistent in a dry atmospheric simulation. If this is the case, it would be of interest to contrast the aforementioned three features of the 30–60-day mode of the atmospheric circulation in the beginning of this section. With this contrast, some light may be shed on the possible effect of the eastward-propagating 30–60-day global divergent circulation on the RAM poleward propagation by the 30–60-day mode and the $\tilde{M}_r$ variation.

Acknowledgements

This study is supported by the NSF Grant ATM-9416954. The typing support provided by Mrs Reatha Diedrichs and the editing assistance by Mr Chris Wikle are highly appreciated.

References

Anderson, J.R., Rosen, R.D., 1983. The latitude–height structure of 40–50 day variations in atmospheric circulation. J. Atmos. Sci. 40, 1584–1591.

Chen, T.-C., Tzeng, R.-Y., Yen, M.-C., 1988. Development and life cycle of the Indian monsoon – effect of the 30–50 day oscillation. Mon. Weather Rev. 116, 2183–2199.

Gutzler, D.S., Madden, R.A., 1993. Seasonal variations of the 40–50 day oscillation in atmospheric angular momentum. J. Atmos. Sci. 50, 850–860.

Kang, I.-S., Lau, K.-M., 1994. Principal modes of atmospheric circulation anomalies associated with global angular momentum fluctuations. J. Atmos. Sci. 51, 1194–1205.

Knutson, T.R., Weickmann, K.M., 1987. 30–60 day atmospheric oscillations: composite life cycles of convection and circulation anomalies. Mon. Weather Rev. 115, 1407–1436.

Krishnamurti, T.N., Jayakumar, D.K., Sheng, J., Surgi, N., Kumar, A., 1985. Divergent circulation on the 30 to 50 day time scale. J. Atmos. Sci. 42, 364–375.

Lambeck, K., Cazenave, A., 1974. The earth's rotation and atmospheric circulation – ii. The continuum. Geophys. J. R. Astron. Soc. 38, 49–61.

Langley, R.G., King, R.W., Shapiro, I.I., Rosen, R.D., Salstein, D.A., 1981. Atmospheric angular momentum and the length of day; a common fluctuation with a period near 50 days. Nature 294, 730–732.

Lorenc, A., 1984. The evolution of plentary scale 200-mb divergence during the FGGE year. Quart. J. Roy. Meteor. Soc., 110, 427–442.

Madden, R.A., Julian, P.R., 1971. Description of a 40–50 day oscillation in the zonal wind in the tropical Pacific. J. Atmos. Sci. 28, 702–708.

Madden, R.A., Julian, P.R., 1972. I. Description of global-scale circulation cells in the tropics with a 40–50 day period. J. Atmos. Sci. 29, 1109–1123.

Madden, R.A., Julian, P.R., 1994. Observations of the 40–50 day tropical oscillation – a review. Mon. Weather Rev. 122, 814–837.

Murakami, M., 1979. Large-scale aspects of deep convective activity over GATE area. Mon. Weather Rev. 107, 997–1013.

Rosen, R.D., 1993. The axial momentum balance of earth and its fluid envelope. Surv. Geophys. 14, 1–29.